version 0

Novel compounds in the Zr-O system, their crystal structures and mechanical properties

Jin Zhang,[1,*] Artem R. Oganov,[1,2,3,†] Xinfeng Li,[4] Huafeng Dong,[1] and Qingfeng Zeng[2]

[1]*Department of Geosciences, Center for Materials by Design, and Institute for Advanced Computational Science, State University of New York, Stony Brook, NY 11794-2100, USA*

[2]*Science and Technology on Thermostructural Composite Materials Laboratory, International Center for Materials Discovery, School of Materials Science and Engineering, Northwestern Polytechnical University, Xi'an, Shaanxi 710072, PR China*

[3]*Moscow Institute of Physics and Technology, Dolgoprudny, Moscow Region 141700, Russia*

[4]*State Key Laboratory for Mechanical Behavior of Materials, School of Materials Science and Engineering, Xi'an Jiaotong University, Xian, 710049, PR China*

Abstract

With the motivation of exploring new high-strength ceramics, ab initio evolutionary simulations are preformed to search for all the stable compounds in the Zr-O system. We have found that not only the traditional compound ZrO_2 is stable at zero pressure, but also ordered suboxides $R\bar{3}$-Zr_6O, $R\bar{3}c$-Zr_3O, $P\bar{3}1m$-Zr_2O and $P\bar{6}2m$-ZrO. The crystal structure of semimetallic $P\bar{6}2m$-ZrO consists of Zr-graphene layers and can be described as an intercalated version of ω-Zr structure. An interesting massive Dirac cone is found in the three-dimensional (3D) band structure of $P\bar{6}2m$-ZrO at the Γ-point. The elastic properties, hardness and the correlation between the mechanical properties of Zr-O compounds and oxygen contents have been systematically investigated. Surprisingly, the hardest zirconium oxide is not ZrO_2, but ZrO. Both $P\bar{6}2m$-ZrO and $P\bar{3}1m$-Zr_2O exhibit relatively high hardnesses of 14 GPa and 10 GPa, respectively. The anisotropic Young's modulus E, torsion shear modulus G_t and linear compressibility β have been derived for $P\bar{6}2m$-ZrO and $P\bar{3}1m$-Zr_2O. Further analyzes of the density of state, band structure and crystal orbital Hamilton population indicate that the electronic structure of Zr-O compounds is directly related to their mechanical properties. The simultaneous occurrence of the 3D-framework of Zr-O and strong Zr-Zr bonds in $P\bar{6}2m$-ZrO explain its high hardness.

I. INTRODUCTION

Zirconia (ZrO_2) is an important modern ceramic material. It can be used as a refractory, a high-κ dielectric, a component in structural ceramics, a substitute for diamond and as an optical material[1,2]. At ambient conditions, it is well known that ZrO_2 has a monoclinic $P2_1/c$ baddeleyite structure, then transforms into orthorhombic-I (*Pbca*, OI) and orthorhombic-II (*Pnma*, OII) phases upon increasing pressure[3,4]. The phase sequence of ZrO_2 at ambient pressure with increasing temperature is as following: baddeleyite $\rightarrow$ tetragonal ZrO_2 ($P4_2/nmc$) $\rightarrow$ cubic ZrO_2 ($Fm3m$, fluorite)[5,6]. A number of theoretical studies of ZrO_2 have been extensively performed[7–9] to understand its electronic, mechanical and structural properties. Zr_3O, which is important for slowing down of hydrogen diffusion inside the bulk of Zr alloy[10], has also been identified at the oxide-metal interface in Zr alloys[11,12]. The closely related Ti-O system has six stable oxide phases: $P31c$-Ti_6O[13], $P\bar{3}1c$-Ti_3O[14], $P\bar{3}m1$-Ti_2O[14], $Fm\bar{3}m$-TiO[15], $R\bar{3}c$-Ti_2O_3[15] and rutile $P4_2mnm$-TiO_2[16], while the Hf-O system has only one known stable phase: monoclinic $P2_1/c$-HfO_2[17] at 0 GPa. Can other compounds be stable in the Zr-O system? In our paper, we focus on searching for stable Zr-O compounds that may have been overlooked at 0 GPa and investigating the hardness trends of these phases.

II. COMPUTATIONAL METHODOLOGY

Searches for stable Zr-O compounds were done using the evolutionary algorithm (EA) as implemented in the USPEX code[18,19] in its variable-composition mode[20], in conjunction with ab initio structure relaxations using density functional theory (DFT) within the PBE-GGA functional[21], as implemented in the VASP package[22]. Evolutionary simulations of the Zr-O system were preformed at 0 GPa with up to 20 atoms in the unit cell. The first generation of Zr-O structures was produced using the random symmetric algorithm[19], all subsequent generations of Zr-O structures were produced in the following manner: 20% were generated randomly, and the rest by variation operators including heredity (40%), lattice mutation (20%), and transmutation (20%). The electron-ion interaction was described by the projector augmented-wave (PAW) pseudopotentials[23], with $4s^24p^65s^24d^2$ and $2s^22p^4$ shells treated as valence for Zr and O, respectively. The plane-wave kinetic energy cutoff was chosen as 600 eV, and we used Γ-centered uniform k-points meshes to sample the

Brillouin zone. A 19×19×19 k-point grid was used to calculate the density of states (DOS). To compute phonons, we used the supercell method as implemented in the Phonopy code[24], and the force constants matrices were computed using 2×2×2 supercells.

III. RESULTS AND DISCUSSIONS

A. Crystal structure prediction and structural properties

The following compounds were found to be thermodynamically stable: $R\bar{3}$-Zr_6O, $R\bar{3}c$-Zr_3O, $P\bar{3}1m$-Zr_2O, $P\bar{6}2m$-ZrO, $P2_1/c$-ZrO_2. Detailed Gibbs free energies of formation of Zr-O compounds under conditions of zero pressure and several temperatures are shown in Fig.1. The hexagonal $P6_3/mmc$-Zr and magnetic solid oxygen were used to generate the convexhull at 0 GPa and 0 K. Our calculations indicated that the known monoclinic $P2_1/c$-ZrO_2 (baddeleyite) is most stable structure for ZrO_2, which is in accordance with the experiment result[25]. Monoclinic ZrO_2 is not only the best known of these compounds, but also exists in the widest range of chemical potentials - unlike Zr_6O, Zr_3O, Zr_2O, ZrO, which are stable only at strongly reducing conditions. This can explain why ZrO_2 is easier to be experimentally observed than other Zr-O compounds. For Zr_3O, the calculated results present here suggest the experimental $R\bar{3}c$-Zr_3O[26] is the most stable structure, which are in agreement with the results of Zr_3O reported by Burton[27]. $P6_322$-Zr_3O (Fe_3N type), which was firstly reported by Holmberg and Dagerhamn[28], exhibits very close but higher formation energy than $R\bar{3}c$-Zr_3O as depicted in Fig. 1(a) (open blue square). Except Holmberg and Dagerhamn[28] proposed the $P6_322$-Zr_3O by means of X-ray diffraction, the $P6_322$-Zr_3O was also confirmed using the neutron diffraction studies by Yamaguchi[29] and Riabov[30], respectively. Our calculated results reveal that no negative frequencies exist in the whole Brillouin zone in the calculated phonon dispersion for $P6_322$-Zr_3O, indicating it is dynamically stable and it should be a metastable phase at 0 K and 0 GPa in the framework of First-Principles DFT calculation. Moreover, we confirmed that $R\bar{3}c$-Zr_3O will transform into $P6_322$-Zr_3O at about 700 K. Therefore the temperature may explain why the experiments were more inclined to find $P6_322$-Zr_3O. $Pn\bar{3}m$-Zr_2O (Cu_2O type) is experimentally reported by Khitrova and Klechkovskays[31]. The formation enthalpy of $Pn\bar{3}m$-Zr_2O is 0.246 eV/atom higher than that of $P\bar{3}1m$-Zr_2O. Coupled with the fact that negative frequencies exist in

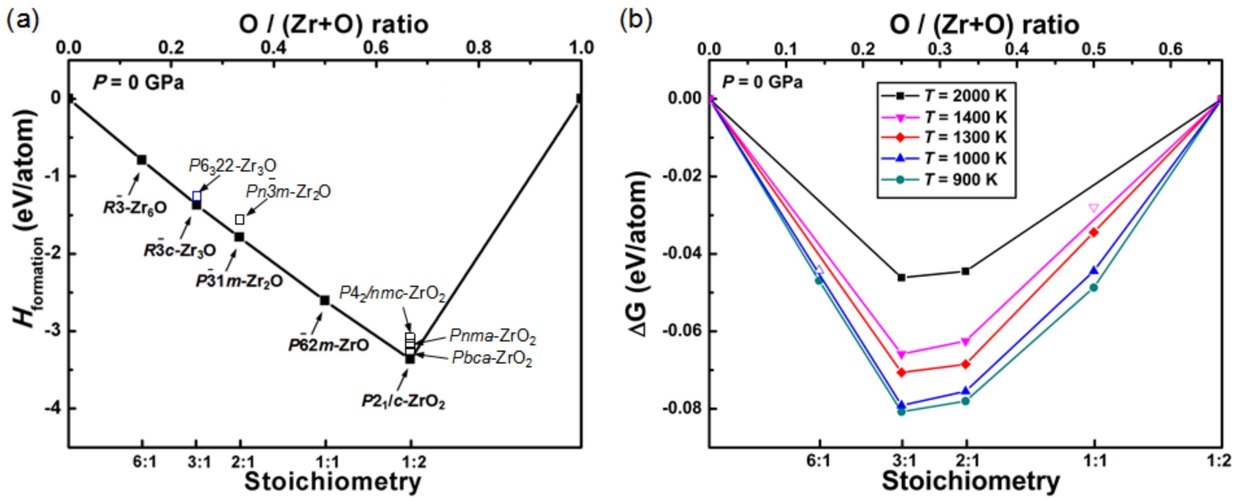

FIG. 1. (a) The enthalpy of formation of Zr-O compounds at 0 GPa and $T = 0$ K. Open squares denote some notable experimental phases. (b) Gibbs free energy of formation for Zr-O compounds at 900 K, 1000 K, 1300 K, 1400 K 2000 K and $P = 0$ GPa (for clarity, the O/(Zr+O) ratio from 0 (Zr) to 0.6667 (ZrO_2) was drawn.). Open triangles represent unstable phases. For the ZrO_2, $P4_2/nmc$-ZrO_2 is used at 2000 K ($P2_1/c$-ZrO_2 will transform into $P4_2/nmc$-ZrO_2 at 1680 K, basically in agreement with the experiment at 1478 K[25]). The Zr_3O shown in (b) should be $P6_322$-Zr_3O since $R\bar{3}c$-Zr_3O will transform into $P6_322$-Zr_3O at about 700 K.

the Brillouin zone of its calculated phonon dispersion, indicating $Pn\bar{3}m$-Zr_2O is an unstable phase at 0 K and 0 GPa.

In order to consider the effects of temperature into formation enthalpy (Fig. 1(b)), quasi-harmonic free-energy of hcp-Zr, Zr_6O, Zr_3O, Zr_2O, ZrO and ZrO_2 were calculated using the Phonopy code[24], while for oxygen we used the expression: $\mu_O(T,p^0) = 1/2[H(T,p^0,O_2)$-$H(0\ K,p^0,O_2)]$-$1/2T[S(T,p^0,O_2)$-$S(0\ K,p^0,O_2)]$[32] to obtain the oxygen chemical potential with 0 K as reference, as shown in Table I. The enthalpy and entropy of O_2 were tabulated in thermochemical tables[33]. We took these values relative to zero Kelvin, and added to them our computed enthalpy of the magnetic O_2 molecule at 0 K (-4.88 eV/atom) to obtain the chemical potential of oxygen as a function of temperature. Except for the ZrO_2 and Zr_3O, Zr_6O, Zr_2O and ZrO did not suffer from the elevated temperature phase transformation.

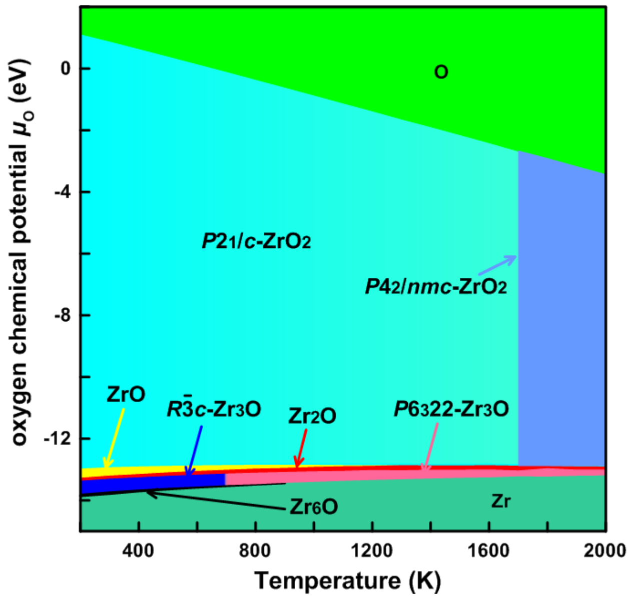

FIG. 2. (Color online) Oxygen chemical potential-temperature phase diagram for Zr-O system.

TABLE I. $\mu_O(T,p^0)$ in the temperature range with 0 K as reference at 1 atm ($\approx$ 0 GPa).

T	$\mu_O(T,p^0)$	T	$\mu_O(T,p^0)$
100 K	-0.07 eV	1100 K	-1.23 eV
200 K	-0.17 eV	1200 K	-1.36 eV
300 K	-0.27 eV	1300 K	-1.49 eV
400 K	-0.38 eV	1400 K	-1.62 eV
500 K	-0.50 eV	1500 K	-1.75 eV
600 K	-0.61 eV	1600 K	-1.88 eV
700 K	-0.73 eV	1700 K	-2.02 eV
800 K	-0.85 eV	1800 K	-2.16 eV
900 K	-0.98 eV	1900 K	-2.30 eV
1000 K	-1.10 eV	2000 K	-2.43 eV

From the convex hulls of the Zr-O system at zero pressure and different temperatures, we have computed the phase diagram of the Zr-O system in axes of temperature and oxygen chemical potential Fig. 2, which can directly visualize the relative stability of these zircon oxides. Note that the region for ZrO_2 in the calculated phase diagram (Fig. 2), our calculations indicate $P2_1/c$-ZrO_2 will transform into $P4_2/nmc$-ZrO_2 at about 1680 K, which

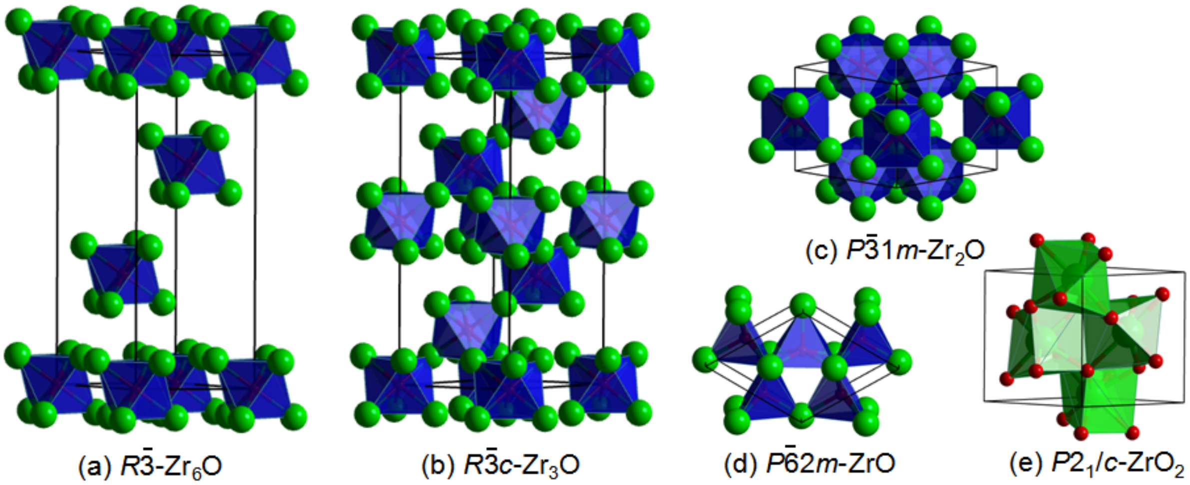

FIG. 3. (Color online) Crystal structures of (a) $R\bar{3}$-Zr_6O (b) $R\bar{3}c$-Zr_3O (c) $P\bar{3}1m$-Zr_2O (d) $P\bar{6}2m$-ZrO (e) $p2_1/c$-ZrO_2. Green spheres-Zr; red spheres-O atoms. O-centered and Zr-centered polyhedra are shown for Zr suboxides and ZrO_2, respectively.

is a little higher than the experimental transition temperature 1478 K[25]. $R\bar{3}c$-Zr_3O will transform into $P6_322$-Zr_3O at about 700 K and continue to be stable as the temperature increasing to 2000 K. It turns out that Zr_6O and ZrO are thermodynamically stable up to 900 K and 1300 K, respectively. Zr_2O is still stable as the temperature increasing up to 2000 K, which is higher than the experimental results 1270 K[25] while is in agreement with the other calculated results[27,34].

Structurally, Zr oxides fall into three groups: intercalated hcp-suboxides (Zr_6O, Zr_3O, Zr_2O), intercalated ω-phase suboxide ZrO, and oxide ZrO_2. Structures of zirconium suboxides Zr_6O, Zr_3O, Zr_2O are based on very similar principles: hexagonal close packing of Zr atoms, in which the O atoms fill 1/6, 1/3, and 1/2 of the octahedral voids, respectively. The O-centered octahedra tend to avoid each other. In the polyhedral representation of the structure of Zr_6O, the O-centered octahedra form "anti-corundum" layers (in these layers, 1/3 of the octahedra are filled by O atoms and 2/3 are empty), which alternate with O-free layers. The structure of Zr_3O is fully built of the "anti-corundum" layers, whereas the structure of Zr_2O displays alternation of "anti-corundum" (with 1/3 filling of the octahedra) and "corundum" layers (with 2/3 filling of the octahedra). One can conjecture that these

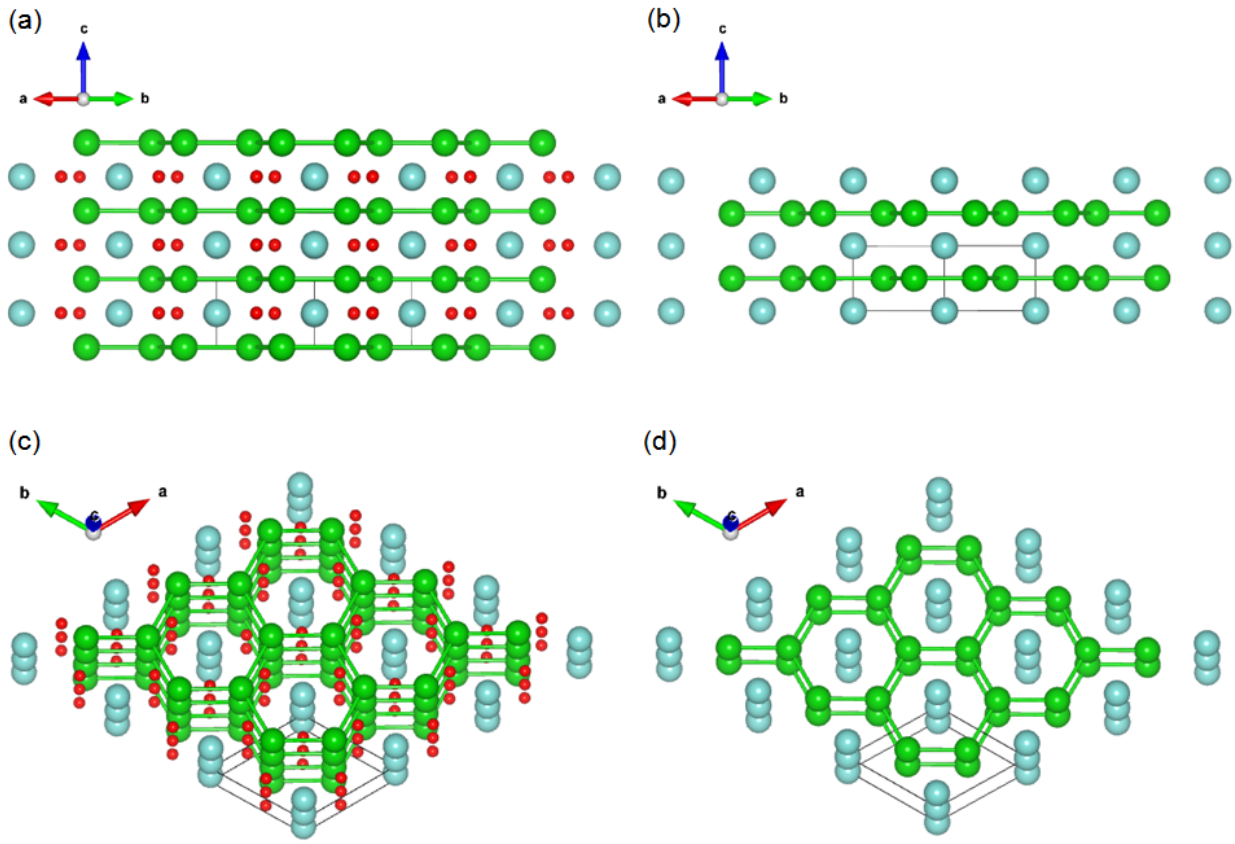

FIG. 4. (Color online) Crystal structures of $P\bar{6}2m$-ZrO (a,c) for comparison ω-Zr (b,d). Green spheres-Zr1; cyan spheres-Zr2; red spheres-O atoms.

suboxides should easily absorb or desorb oxygen, transforming into one another without loss of single-crystallinity.

The structure of ZrO is rather unusual - it consists of Zr-graphene layers (Fig. 3(c)) stacked on top of each other (Zr-Zr distances within the layer are 3.08 Å, and between the layers 3.22 Å), as illustrated in Fig. 4(a). In the center of the big hexagonal void between the two graphene layers, there is an additional Zr atom surrounded by three oxygens (Zr-O distance 2.16 Å), and each of these oxygens is also bonded to four other Zr atoms (at distances 2.28 Å). This structure, therefore, is built by a 3D-framework of short and strong

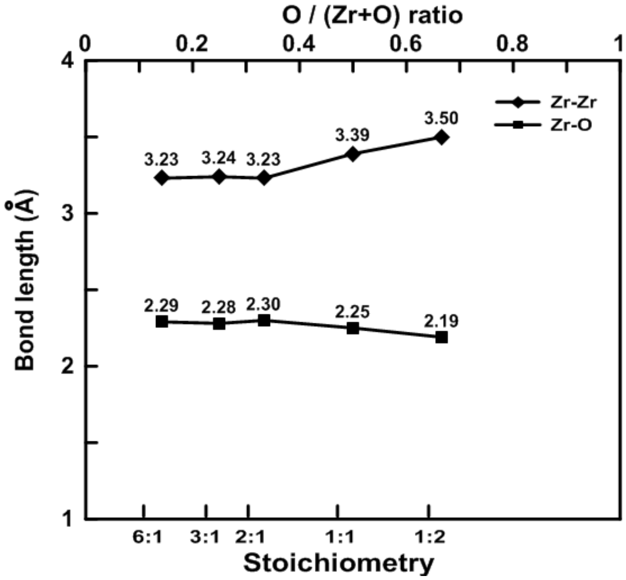

FIG. 5. Average bond lengths in Zr-O compounds.

Zr-O bonds, reinforced by rather strong Zr-Zr bonds. The former lead to high hardness, the latter may improve toughness due to semimetallic behavior. Moreover, the crystal structure of $P\bar{6}2m$-ZrO shares significant features with the structure of the well known phase ω-Zr. The ω phase has been observed in some Ti, Zr and Hf-based alloys[35,36]. ω-Zr with space group $P6/mmm$ is the high pressure allotrope of α-Zr (hcp structure, space group $P6_3/mmc$). ω-Zr has an interesting crystal structure related to the AlB_2 structure type; it has three atoms per unit cell and cell parameters a = 5.036, c = 3.109[37] (c = 3.136[38]). The Zr atoms in both $P\bar{6}2m$-ZrO and ω-Zr have the same arrangement as atoms of Al and B in the AlB_2 structure, see Fig. 4. Xue et al. predicted that $P\bar{4}m2$-Zr_2O_3[39] is stable; however, we find that this phase is not energetically favorable at 0 GPa. It turns out to be metastable with respect to decomposition into $P\bar{6}2m$-ZrO and $P2_1/c$-ZrO_2 at 0 GPa. The weighted average lengths of Zr-Zr and Zr-O bonds in Zr-O compounds are plotted in Fig. 5.

Table II lists the detailed crystallographic data of Zr-O compounds at 0 GPa. Our variable-composition USPEX calculations reveal that the Zr-O binary system has five stable compounds ($R\bar{3}$-Zr_6O, $R\bar{3}c$-Zr_3O, $P\bar{3}1m$-Zr_2O, $P\bar{6}2m$-ZrO and $P2_1/c$-ZrO_2), see Fig. 1. Among these, $R\bar{3}$-Zr_6O, $P\bar{3}1m$-Zr_2O, $P\bar{6}2m$-ZrO are hitherto unknown compounds. The structural stability of these novel Zr-O compounds has been checked by phonon calculations.

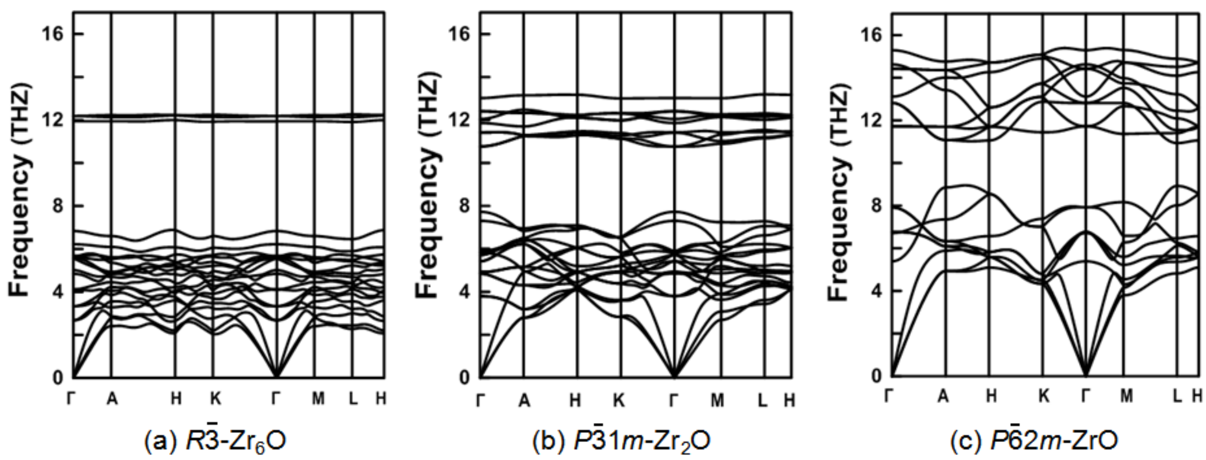

FIG. 6. Phonon dispersions of (a) $R\bar{3}$-Zr_6O (b) $P\bar{3}1m$-Zr_2O (c) $P\bar{6}2m$-ZrO at 0 GPa.

As shown in Fig. 6, no imaginary phonon frequencies are detected throughout the Brillouin zone, indicating that these structures are all dynamically stable. It is notable that the vibrations of O atoms in the suboxides are decoupled from lattice modes, as shown in Fig. 5.

B. Mechanical properties of the Zr-O system

The elastic constants of $R\bar{3}$-Zr_6O , $R\bar{3}c$-Zr_3O, $P\bar{3}1m$-Zr_2O, $P\bar{6}2m$-ZrO and $P2_1/c$-ZrO_2 are summarized in Table III. From the elastic constants, we have ascertained that all these phases satisfy the mechanical stability criteria[40–42].

Compositional variations of the bulk (B), shear (G), Young's (E) moduli, G/B ratio, Poisson' ratio ν and hardness (H_v) of $R\bar{3}$-Zr_6O, R-$\bar{3}c$-Zr_3O, $P\bar{3}1m$-Zr_2O, $P\bar{6}2m$-ZrO, $P2_1/c$-ZrO_2 are displayed in Fig. 7. When the ratio of O/(Zr+O) is 0.5, i.e. for ZrO, the mechanical properties B, G, E, G/B and hardness reach the peak values while the ν value is minimum, as listed in Table III. The large c_{33} values indicate that all the Zr-O compounds are highly incompressible along the c axis. The magnitude of variation in G and B is very large, as G and B values vary in ranges 40-120 GPa and 110-200 GPa, respectively. The criterion proposed by Pugh[44] and the Poisson' ratio ν can be used to evaluate the brittle/ductile behavior of isotropic materials. According to Pugh's criterion, a material is brittle if $G/B > 0.57$. It seems natural to extend this criterion and expect that higher the value of G/B, the more brittle the materials would be. In the case of $G/B < 0.57$, a material is ductile.

TABLE II. Structural parameters of Zr-O compounds found by USPEX at ambient pressure.

Compound	Space group	Enthalpy of formation (eV/atom)	Lattice constants (Å)	Wyckoff positions	x	y	z
Zr_6O	$R\bar{3}$	-0.79	a=5.65	Zr 18f	0.337	0.003	0.419
			c=15.64	O 3a	0.00	0.00	0.00
Zr_3O	$R\bar{3}c$	-1.73	a=5.674	Zr 18e	0.326	0.993	0.083
			c=15.697	O 6b	0.00	1.00	0.00
Zr_2O	$P\bar{3}1m$	-1.78	a=5.654	Zr 6k	0.333	1.00	0.253
			c=5.248	O 2c	0.333	0.667	0.00
				O 1b	0.00	1.00	0.50
ZrO	$P\bar{6}2m$	-2.61	a=5.327	Zr 1b	0.00	1.00	0.50
			c=3.218	Zr 2c	0.6667	0.333	0.00
				O 3g	0.406	0.00	0.50
ZrO_2	$P2_1/c$	-3.36	a=5.220	Zr 4e	0.276	0.0436	0.710
			b=5.280	O 4e	0.067	0.329	0.848
			c=5.407	O 4e	0.450	0.757	0.976
			$\beta = 99.67°$				

The calculation, as shown in Fig. 7(d,e), reveal that Zr_6O is more ductile than the other Zr-O compounds. In addition, the hardness comparison is drawn between $P6_322$-Zr_3O (a commonly experimental phase we mention above) and $R\bar{3}c$-Zr_3O: it turns out that the hardness of $P6_322$-Zr_3O is 5 GPa, which is similar with the hardness of $R\bar{3}c$-Zr_3O. The Vickers hardness was calculated according to Chen's model[45]:

$$H_V = 2 * (k^2 * G)^{0.585} - 3 \quad (1)$$

Once again, and surprisingly, we find that ZrO has the highest hardness, see Fig. 7(f). Combined with the Fig. 7(a), (b) and (c), we can also conclude that incorporation of oxygen interstitials improves hardness and increases brittleness, which is consistent with experimental results[46,47]. However, we find it a big surprise that ZrO is harder than ZrO_2.

TABLE III. Calculated elastic constants C_{ij}, bulk modulus B, shear modulus G, Young's modulus E, Poisson's ratio υ, hardness of Zr−O compounds and some literature values of ZrO_2. All properties are in GPa (except dimensionless G/B and υ).

					ZrO_2		
Compound	Zr_6O	Zr_3O	Zr_2O	ZrO	This work	Calc.[9]	Expt.[43]
c_{11}	162	201	269	330	301	337	361
c_{22}					354	351	408
c_{33}	207	217	283	347	253	268	258
c_{44}	50	71	96	125	73	79	99.9
c_{55}					81	70	81.2
c_{66}					117	114	126
c_{12}	97	106	110	102	154	155	142
c_{13}	72	92	100	136	96	84	55
c_{14}	-3.3	16	-19				
c_{15}	8				40	26	-21.3
c_{23}					146	153	196
c_{25}					-4	-4	31.2
c_{35}					1.5	1.9	-18.2
c_{45}					-8	-14.6	-22.7
B_H	112	133	160	195	182	189	190
G_H	44	58	86	115	85	87	96
E	114	151	219	288	220	227	247
G/B	0.39	0.4	0.54	0.59	0.47	0.46	0.50
υ	0.33	0.3	0.27	0.25	0.3	0.3	0.28
H_V	3	5	10	14	7.9	8.1	10

We further investigated the elastic anisotropy of $P\bar{6}2m$-ZrO (the hightest bulk modulus, shear modulus and hardness among Zr-O compounds) and $P\bar{3}1m$-Zr_2O (the second hardest Zr-O compound), Young's modulus, torsion shear modulus and linear compressibility. The directional dependence of the Young's modulus for hexagonal and trigonal crystals can be calculated as:

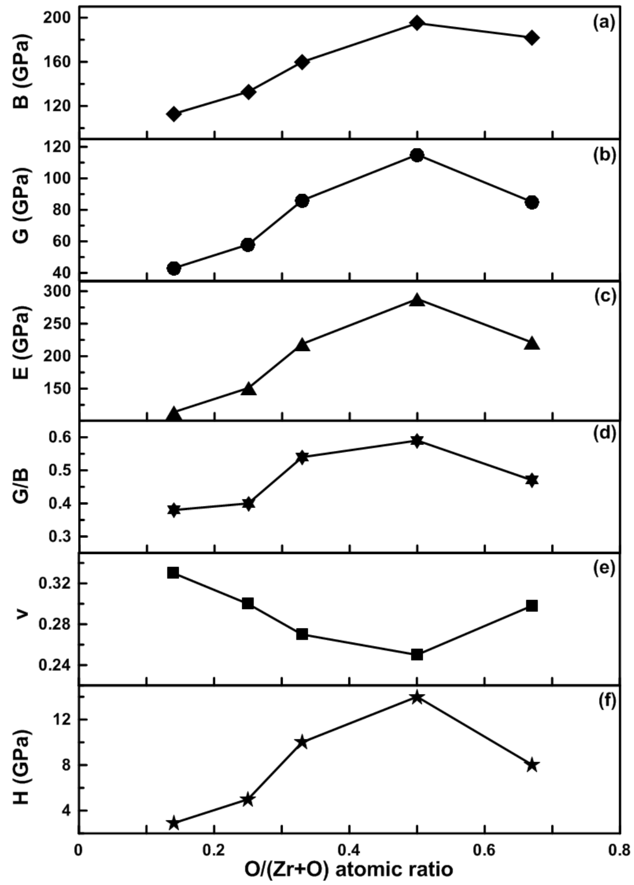

FIG. 7. Variation of B, G, E, G/B, υ and H with increasing O contents in Zr-O compounds.

$$\frac{1}{E_{hex}} = s_{11}(1-l_3^2)^2 + s_{33}l_3^4 + (2s_{13}+s_{44})l_3^2(1-l_3^2) \tag{2}$$

$$\frac{1}{E_{tri}} = (1-l_3^2)s_{11} + l_3^4 s_{33} + l_3^2(1-l_3^2)(2s_{13}+s_{44}) + 2l_2l_3(3l_1^2-l_2^2)s_{14}, \tag{3}$$

where s_{11}, s_{12}, etc., are the elastic compliance constants and l_1, l_2, l_3 are the direction cosines of a particular crystallographic orientation to coordinate axes x_1, x_2 and x_3, respectively.

To understand deeper the elasticity, as well as plastic deformation and crack behavior in $P\bar{6}2m$-ZrO and $P\bar{3}1m$-Zr_2O, it is necessary to study the dependence of the shear modulus on stress direction. However, the shear modulus varies not only with the shear plane but also with the direction within that plane. Therefore, it is impossible to draw three-dimensional images to directly visualize the orientation-dependent shear modulus. Shear modulus is often measured by torsion shear modulus, which is an average in the shear plane, and it is

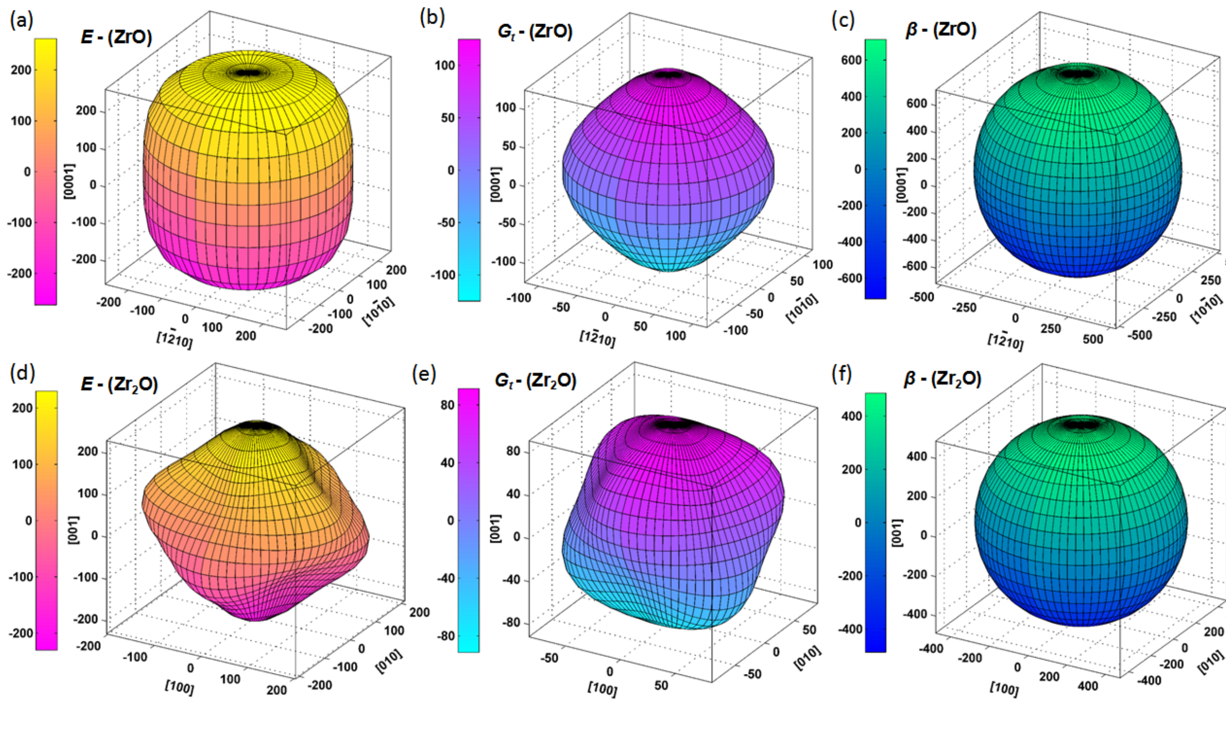

FIG. 8. The orientation dependence of Young's moduli (in GPa) for (a) $P\bar{6}2m$-ZrO and (d) $P\bar{3}1m$-Zr_2O. Directional dependence of the torsion shear moduli (in GPa) for (b) $P\bar{6}2m$-ZrO and (e) $P\bar{3}1m$-Zr_2O. Anisotropy of the linear compressibility (in Å) for (c) $P\bar{6}2m$-ZrO and (f)$P\bar{3}1m$-Zr_2O.

only related to the direction of the shear plane and can be represented by three-dimensional diagrams. The torsion shear modulus (G_t) along an arbitrary direction can be calculated for hexagonal and trigonal crystals as follows:

$$\frac{1}{G_{t(hex)}} = s_{44} + [(s_{11} - s_{12}) - \frac{1}{2}s_{44}](1 - l_3^2) + 2(s_{11} + s_{33} - 2s_{13} - s_{44})l_3^2(1 - l_3^2) \quad (4)$$

and

$$\begin{aligned} \frac{1}{G_{t(tri)}} =& s_{11}(3l_1^2 - 2l_1^4 - 2l_2^4 + 3l_2^2 - 4l_1^2l_2^2) + 2s_{33}l_3^2(1 - l_3^2) \\ &+ \frac{1}{2}s_{44}(l_1^2 + l_2^2 + 2l_3^2 - 4l_2^2l_3^2 - 4l_1^2l_3^2) - s_{12}(l_1^2 + l_2^2) \\ &- 4s_{13}l_3^2(l_1^2 + l_2^2) + 2s_{14}(2l_2^3l_3 - 5l_1^2l_2l_3 - l_1^2l_2l_3) \end{aligned} \quad (5)$$

The linear compressibility of a crystal is the relative decrease in length of a line when the crystal is subjected to unit hydrostatic pressure. In general it is anisotropic. For both hexagonal and trigonal systems, the directional dependence of linear compressibility β can be expressed as

$$\beta = (s_{11} + s_{12} + s_{13}) - (s_{11} + s_{12} - s_{13} - s_{33})l_3^2 \quad (6)$$

As shown in Fig. 8, both P$\bar{3}$1m-Zr_2O and $P\bar{6}2m$-ZrO exhibit a moderate amount of anisotropy of these quantities.

C. Chemical bonding in the Zr-O system

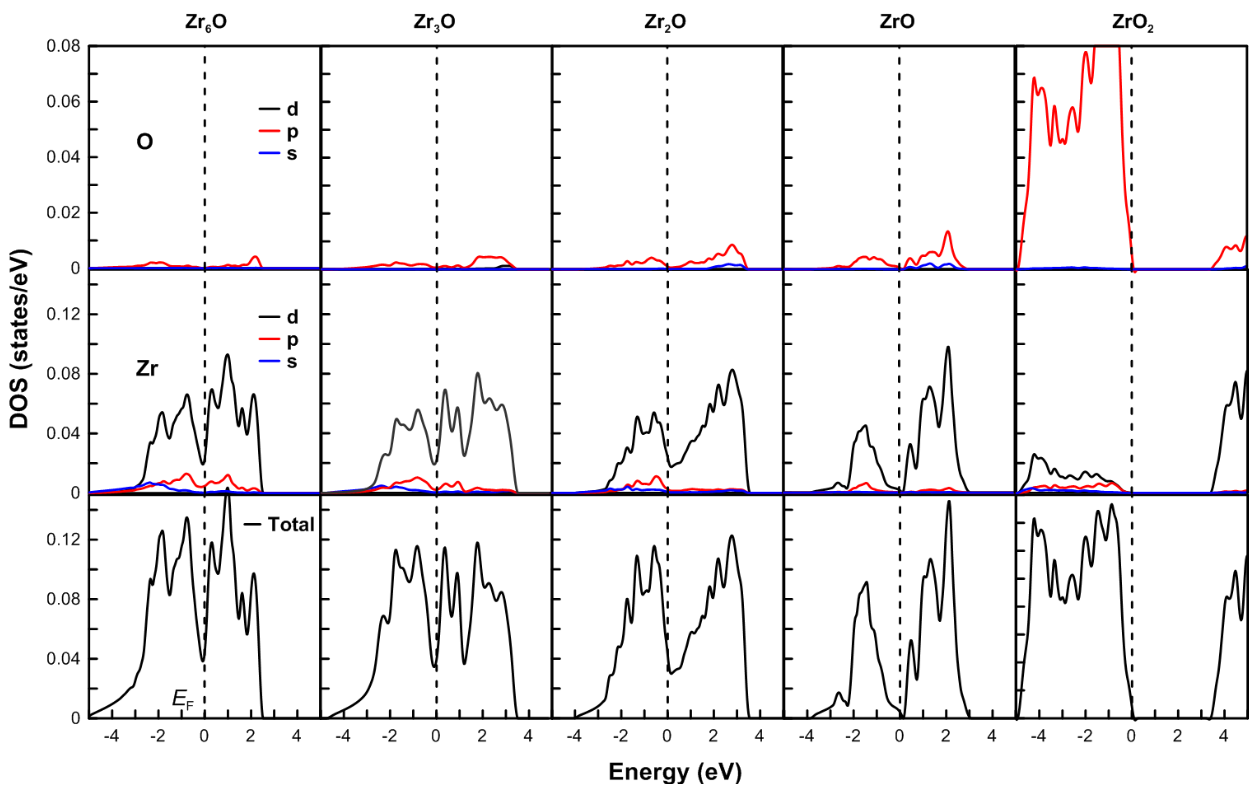

FIG. 9. (Color online) The normalized (per electron) total and partial densities of states for (a) $R\bar{3}$-Zr_6O (b) $R\bar{3}c$-Zr_3O (c) $P\bar{3}1m$-Zr_2O (d) $P\bar{6}2m$-ZrO (e) $P2_1/c$-ZrO_2. The Fermi energy is set to zero.

Total and partial densities of states (DOS) are presented in Fig. 9. For the total DOS of Zr_6O, Zr_3O and Zr_2O, there is no band gap in the DOSs at the Fermi level (E_F), indicating that these compounds are metals. A sharp valley (pseudogap) around the Fermi energy is a typical feature of the borderline between the bonding and antibonding states and an indication of electronic stabilization[48–51]. ZrO_2 is obviously an insulator with a wide band gap. Interestingly and unlike the other compounds, ZrO is a semimetal with very few states at the Fermi level. The DOSs of Zr_6O, Zr_3O and Zr_2O below E_F are mainly contributed by the Zr-d, Zr-p and O-p orbitals and the interactions between the Zr-d occupied orbitals are responsible for metallicity. The highest occupied states in ZrO_2 are derived mainly from O-p orbitals. In addition, the valence band of Zr_6O, Zr_3O,Zr_2O and ZrO shown in Fig. 8 gradually shrinks with increasing O content. Valence band width reaches minimum for ZrO.

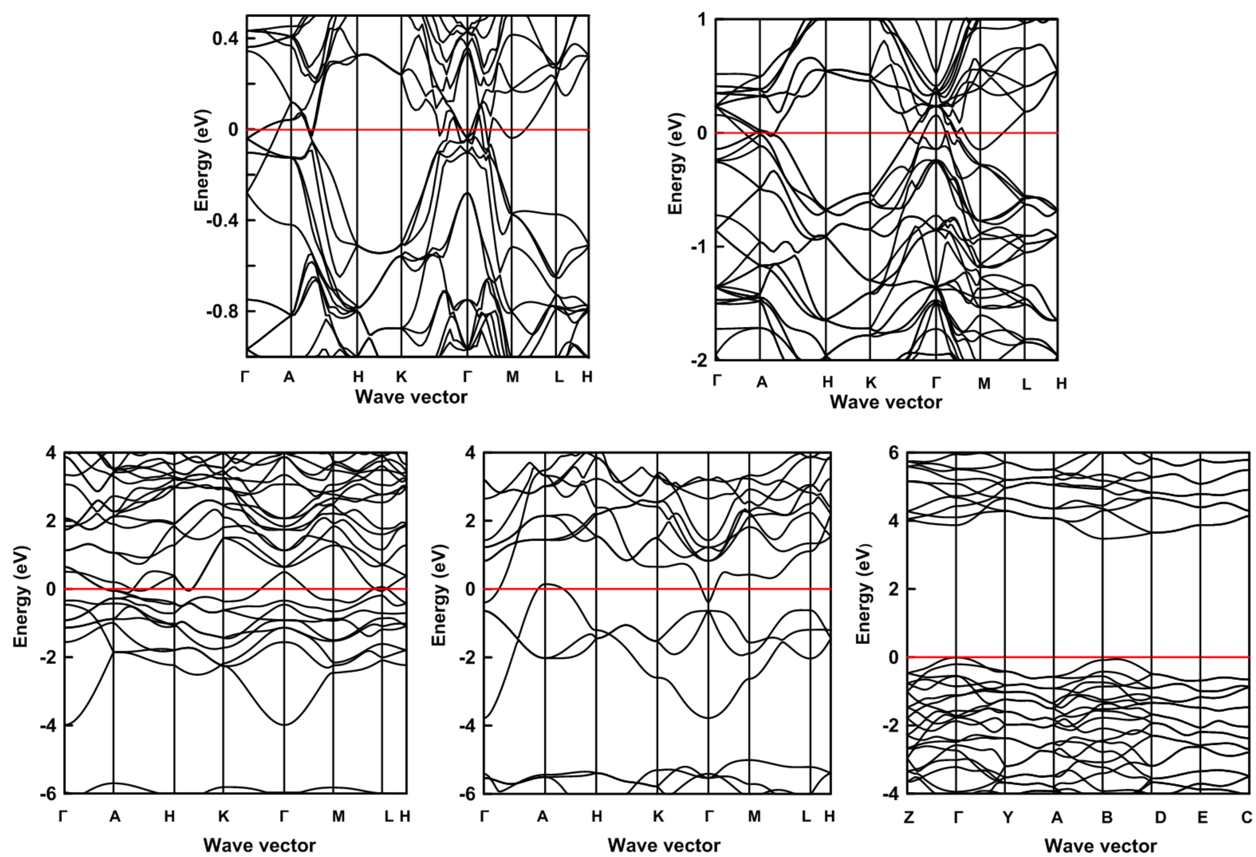

FIG. 10. (Color online) Band structures of (a) $R\bar{3}$-Zr_6O (b) $R\bar{3}c$-Zr_3O (c) $P\bar{3}1m$-Zr_2O (d) $P\bar{6}2m$-ZrO (e) $P2_1/c$-ZrO_2. The Fermi energy is set to zero.

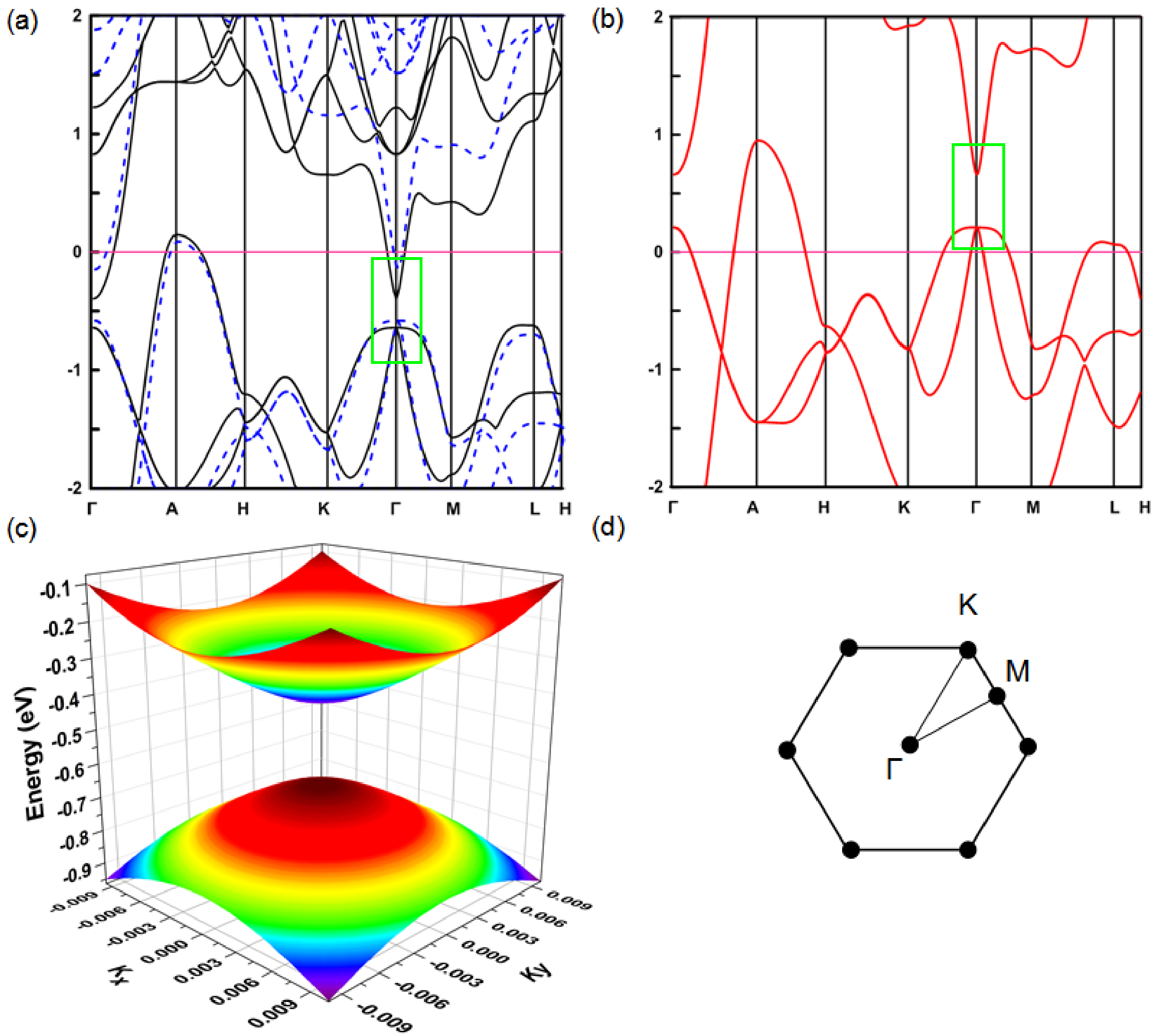

FIG. 11. (Color online) Electronic structure of $P\bar{6}2m$-ZrO in (a) DFT-GGA (black lines) and HSE06 (blue dashed lines), (b) GW (red solid lines). The Fermi energy is set to zero. (c) Dirac cone formed by the valence and conduction bands in the vicinity of the Dirac point. (d) First Brillouin zone with special k points: Γ(0 0 0), K(-0.333 0.667 0), M(0 0.5 0).

Fig. 10 shows band structures of Zr-O compounds. As shown in Fig. 11(a,b), semimetallic character[39] of $P\bar{6}2m$-ZrO is very clear (the overlap of the partially occupied valence band top and conduction band bottom located at the different high symmetry points A and Γ, respectively) in DFT and was confirmed by calculations using the hybrid functional

HSE06 and GW approximation, respectively. We have also confirmed that semimetallicity of $P\bar{6}2m$-ZrO remains unchanged at positive and negative strains. One can observe that a very interesting massive Dirac-cone exists at the Γ-point, as shown in the green rectangle (Fig. 11(a)), slightly below (in the GGA and HSE06) or slightly above (in GW) the Fermi level. The 3D Dirac cone in the vicinity of Γ-point is displayed in Fig. 10(c).

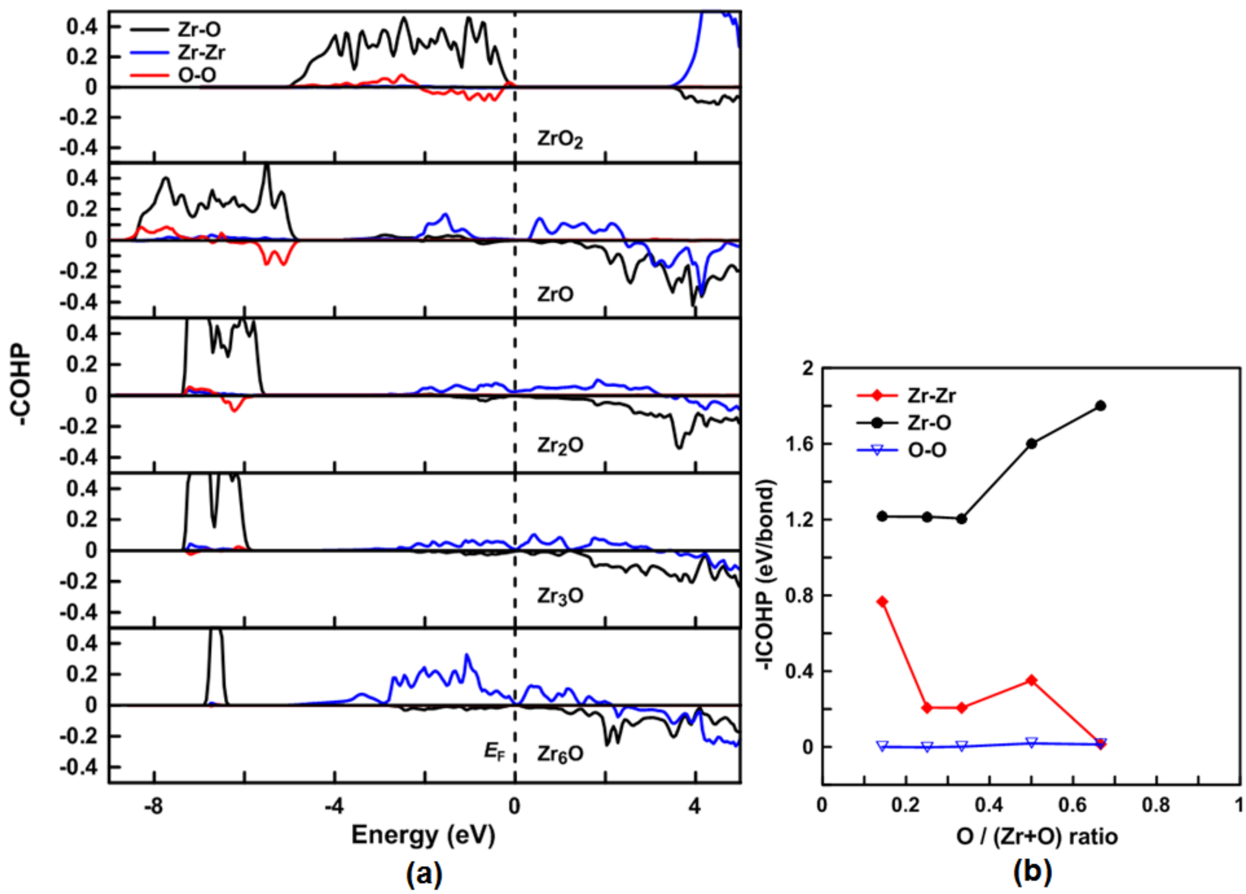

FIG. 12. (a) Crystal orbital Hamilton population (COHP) curves for Zr-O compounds. The dotted line at zero is the Fermi level. (b) The calculated integrated crystal orbital Hamiltonian populations (-ICOHP) for Zr-Zr, Zr-O and O-O interactions in Zr-O compounds.

To identify the bonding and anti-bonding interactions in the Zr-O compounds, we have calculated the crystal orbital Hamilton populations (COHP) and integrated crystal orbital Hamilton populations (ICOHP)[52] using the TB-LMTO-ASA program[53]. Bonding states indicated by negative values and anti-bonding states indicated by positive values (for convenience, we plot -COHP and -ICOHP, where bonding is indicated by positive values) are easy to observe in Fig. 12(a). Clearly, (1) the strength of Zr-Zr interactions falls rapidly with increasing O content, (2) peculiar and unique among these compounds combination of strong Zr-Zr and Zr-O bonding interactions in ZrO explains its superior mechanical properties.

IV. CONCLUSIONS

We have systematically searched the crystal structures of Zr-O system at 0 GPa using ab intio evolutionary algorithm USPEX. Three new stable compounds have been found, namely $R\bar{3}$-Zr_6O, $P\bar{3}1m$-Zr_2O and $P\bar{6}2m$-ZrO. Our results demonstrate that Zr_6O is more ductile than other zirconium oxides, while ZrO is the hardest one. The electronic structure of Zr_6O, Zr_3O,Zr_2O and ZrO shows that the disappearance of ductile Zr-Zr metallic bond and the occurrence of Zr-O bonds are responsible for the increasing hardness. The peculiar combination of strong Zr-O and Zr-Zr bonds in $P\bar{6}2m$-ZrO enables it to have superior mechanical properties, such as bulk modulus B, shear modulus G, Young's modulus E and hardness H_v. The recognition of the common structural features between $P\bar{6}2m$-ZrO and ω-Zr gives further insight into the physical properties and suggests that ZrO can be made as a hard semimetallic coating on ω-Zr substrate.

ACKNOWLEDGMENTS

The authors thank Xiang-Feng Zhou (Stony Brook University) and Qing-Gao Wang (Moscow Institute of Physics and Technology) for valuable discussion. This work was supported by the National Science Foundation (EAR-1114313, DMR-1231586), DARPA (Grants No. W31P4Q1310005 and No. W31P4Q1210008), the Basic Research Foundation of NWPU (No. JCY20130114), the Natural Science Foundation of China (No. 51372203, 51332004), the Foreign Talents Introduction, the Academic Exchange Program of China (No. B08040) and the Government (No. 14.A12.31.0003) of Russian Federation. The computational resources at High Performance Computing Center of NWPU are also gratefully acknowledged.

---

* Jin.Zhang.1@stonybrook.edu

† artem.oganov@stonybrook.edu

[1] D. Baghmar, Phase Transitions **86**, 811 (2013).

[2] J. K. Dewhurst and J. E. Lowther, Phys. Rev. B **57**, 741 (1998).

[3] S. Desgreniers and K. Lagarec, Phys. Rev. B **59**, 8467 (1999).

[4] M. H. Manghnani and T. Yagi, *Properties of earth and planetary materials at high pressure and temperature*, Vol. 101 (American Geophysical Union, 1998).

[5] G. Teufer, Acta Crystallographica **15**, 1187 (1962).

[6] D. K. SMITH and C. F. CLINE, Journal of the American Ceramic Society **45**, 249 (1962).

[7] H. Jiang, R. I. Gomez-Abal, P. Rinke, and M. Scheffler, Phys. Rev. B **81**, 085119 (2010).

[8] Y. J. Hao, L. Zhang, X. R. Chen, L. C. Cai, Q. Wu, and D. Alfè, Phys. Rev. B **78**, 134101 (2008).

[9] G. Fadda, L. Colombo, and G. Zanzotto, Phys. Rev. B **79**, 214102 (2009).

[10] M. V. Glazoff, A. Tokuhiro, S. N. Rashkeev, and P. Sabharwall, J. Nucl. Mater. **444**, 65 (2014).

[11] T. Ericsson, G. Östberg, and B. Lehtinen, J. Nucl. Mater. **25**, 322 (1968).

[12] A. Yilmazbayhan, E. Breval, A. T. Motta, and R. J. Comstock, J. Nucl. Mater. **349**, 265 (2006).

[13] S. Yamaguchi, M. Koiwa, and M. Hirabayashi, J. Phys. Soc. Jpn. **21**, 2096 (1966).

[14] I. Kornilov, V. Vavilova, L. Fykin, R. Ozerov, S. Solowiev, and V. Smirnov, Metall. Trans. **1**, 2569 (1970).

[15] D. A. Andersson, P. A. Korzhavyi, and B. Johansson, Phys. Rev. B **71**, 144101 (2005).

[16] J. Muscat, V. Swamy, and N. M. Harrison, Phys. Rev. B **65**, 224112 (2002).

[17] J. M. Leger, A. Atouf, P. E. Tomaszewski, and A. S. Pereira, Phys. Rev. B **48**, 93 (1993).

[18] A. R. Oganov and C. W. Glass, J. Chem. Phys. **124**, 244704 (2006).

[19] A. O. Lyakhov, A. R. Oganov, H. T. Stokes, and Q. Zhu, Comput. Phys. Commun. **184**, 1172 (2013).

[20] A. R. Oganov, A. O. Lyakhov, and M. Valle, Acc. Chem. Res. **44**, 227 (2011).

[21] J. P. Perdew, K. Burke, and M. Ernzerhof, Phys. Rev. Lett. **77**, 3865 (1996).

[22] G. Kresse and J. Furthmüller, Phys. Rev. B **54**, 11169 (1996).

[23] P. E. Blöchl, Phys. Rev. B **50**, 17953 (1994).

[24] A. Togo, F. Oba, and I. Tanaka, Phys. Rev. B **78**, 134106 (2008).

[25] J. Abriata, J. Garces, and R. Versaci, Bulletin of Alloy Phase Diagrams **7**, 116 (1986).

[26] A. Dubertret and P. Lehr, Sci. Park, S6rie C **267**, 820 (1968).

[27] B. Paul Burton, A. van de Walle, and H. T. Stokes, Journal of the Physical Society of Japan **81** (2011).

[28] B. Holmberg and T. Dagerhamn, Acta Chem. Scand **15**, 14 (1961).

[29] S. Yamaguchi, Journal of the Physical Society of Japan **24**, 855 (1968).

[30] A. Riabov, V. Yartys, B. Hauback, P. Guegan, G. Wiesinger, and I. Harris, Journal of alloys and compounds **293**, 93 (1999).

[31] V. Khitrova and V. Klechkovskaya, (1985).

[32] K. Reuter and M. Scheffler, Phys. Rev. B **65**, 035406 (2001).

[33] D. R. Stull and H. Prophet, *JANAF thermochemical tables*, Tech. Rep. (DTIC Document, 1971).

[34] B. Puchala and A. Van der Ven, Physical Review B **88**, 094108 (2013).

[35] S. Sikka, Y. Vohra, and R. Chidambaram, Prog. Mater. Sci. **27**, 245 (1982).

[36] B. Hatt, J. Roberts, and G. Williams, Nature **180**, 1406 (1957).

[37] J. C. Jamieson, Science **140**, 72 (1963).

[38] M. T. Pérez-Prado, A. Gimazov, O. A. Ruano, M. Kassner, and A. Zhilyaev, Scripta Mater. **58**, 219 (2008).

[39] K. H. Xue, P. Blaise, L. R. C. Fonseca, and Y. Nishi, Phys. Rev. Lett. **110**, 065502 (2013).

[40] R. Cowley, Phys. Rev. B **13**, 4877 (1976).

[41] A. Y. Liu and R. M. Wentzcovitch, Phys. Rev. B **50**, 10362 (1994).

[42] B. Karki, G. Ackland, and J. Crain, J. Phys.: Condens. Matter **9**, 8579 (1997).

[43] S. K. Chan, Y. Fang, M. Grimsditch, Z. Li, M. V. Nevitt, W. M. Robertson, and E. S. Zouboulis, J. Am. Ceram. Soc. **74**, 1742 (1991).

[44] S. Pugh, Philos. Mag. **45**, 823 (1954).

[45] X. Q. Chen, H. Niu, D. Li, and Y. Li, Intermetallics **19**, 1275 (2011).

[46] A. Dubertret and P. Lehr, CR Acad. Hebd. Sances Sci. **263**, 591 (1966).

[47] A. W. Cronenberg and M. S. El-Genk, J. Nucl. Mater. **78**, 390 (1978).

[48] J. H. Xu and A. J. Freeman, Phys. Rev. B **41**, 12553 (1990).

[49] J. K. Burdett, E. Canadell, and G. J. Miller, JACS **108**, 6561 (1986).

[50] X. B. Wang, D. C. Tian, and L. L. Wang, J. Phys.: Condens. Matter **6**, 10185 (1994).

[51] P. Vajeeston, P. Ravindran, C. Ravi, and R. Asokamani, Phys. Rev. B **63**, 045115 (2001).

[52] R. Dronskowski and P. E. Bloechl, J. Phys. Chem. **97**, 8617 (1993).

[53] G. Krier, O. Jepsen, A. Burkhardt, and O. Andersen, Stuttgart, April (1995).